

## From benzobisthiadiazole, thiadiazoloquinoxaline to pyrazinoquinoxaline based polymers: effects of aromatic substituents on the performance of organic photovoltaics†

Teck Lip Dexter Tam,<sup>ab</sup> Teddy Salim,<sup>ab</sup> Hairong Li,<sup>b</sup> Feng Zhou,<sup>b</sup> Subodh G. Mhaisalkar,<sup>ab</sup> Haibin Su,<sup>b</sup> Yeng Ming Lam<sup>\*ab</sup> and Andrew C. Grimsdale<sup>\*ab</sup>

Received 24th May 2012, Accepted 13th July 2012

DOI: 10.1039/c2jm33317a

Here we report the syntheses of low bandgap polymers based on benzobisthiadiazole (BBT), thiadiazoloquinoxaline (TQ) and pyrazinoquinoxaline (PQ) core structures with different aromatic substituents. The effects of changing core structures from BBT to PQ and also substituents from biphenyl and bithienyl on the photophysical, electrochemical and morphology of the polymers were studied. These polymers were incorporated into solar cell devices as donors, with PC[71]BM as acceptors, and their device performances were correlated with their properties. It was found that the effect of these structural changes has significant consequences on the overall device performances.

## Introduction

Low bandgap polymers are of interest in current organic photovoltaic (OPV) research as high power conversion efficiency may be achieved from bulk heterojunction (BHJ) devices using them as electron donors.<sup>1–4</sup> Ideally, the materials used should have broad absorption spectra to ensure effective harvesting of the solar photons.<sup>2,5–7</sup> In designing low bandgap polymers, the more common strategies involve using (1) alternating donor–acceptor units to induce intramolecular charge transfer and (2) the introduction of pro-quinoid units which promote quinoid character along the backbone.<sup>8,9</sup> The main strategy used in designing polymers with broad absorption spectra, on the other hand, involves attaching conjugated side chains to the polymer main chains.<sup>10–13</sup> To date, there is no report on the combined use of all three strategies to achieve low bandgap and broad absorption polymers.

Previously, we have reported the synthesis of benzo[1,2-*c*:4,5-*c'*]bis[1,2,5]thiadiazole (BBT), [1,2,5]thiadiazolo[3,4-*g*]quinoxaline (TQ) and pyrazino[2,3-*g*]quinoxaline (PQ) based small molecules that show low bandgaps and broad absorption ranges.<sup>14</sup> While the low bandgap character of the BBT derivative is due to the strong intramolecular charge transfer and quinoid character within the molecule, the broad absorption range of the

TQ and PQ molecules is a consequence of their possessing conjugated side chains. A number of low bandgap polymers containing BBT, TQ and PQ units have been reported, some of which have shown promising results in OPV devices.<sup>15–23</sup> In this paper, we report the synthesis of copolymers of these units with fluorene and their testing as donor materials in BHJ OPV devices. The effect of the conjugated side chains on these polymers upon their performance in OPV devices is discussed.

## Results and discussion

## Polymer syntheses

Compounds **1**, **2**, **3**, **4**, **PQ1** and **PQ2** were synthesized as previously reported.<sup>14,24</sup> **1** was combined with the tin reagent **2** by Stille coupling to yield the polymer **pBBTF**. For the syntheses of TQ polymers, **1** was partially reduced using iron in acetic acid, followed by condensation with diketone **3** or **4** to yield the dibromo TQ derivatives **5** and **6** respectively. Stille coupling of

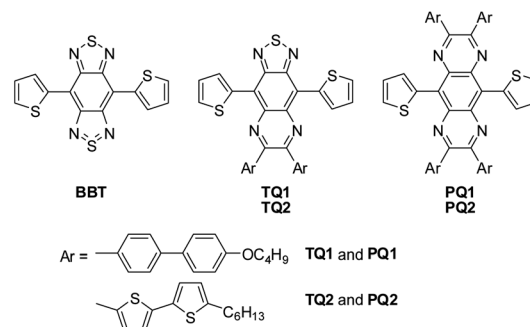


Fig. 1 Structures of the monomer units.

<sup>a</sup>Energy Research Institute @ NTU (ERI@N), Nanyang Technological University, 50 Nanyang Drive, Singapore 637553. E-mail: ymlam@ntu.edu.sg; ACGrimsdale@ntu.edu.sg

<sup>b</sup>School of Materials Science and Engineering, Nanyang Technological University, 50 Nanyang Avenue, Singapore 639798

† Electronic supplementary information (ESI) available: Detailed syntheses of all new compounds, structures of **PQ1a** and **PQ2a**, NMR and MALDI-TOF of all new intermediates, and NMR, TGA, DSC and CV of all polymers. See DOI: 10.1039/c2jm33317a

**Table 1** Characterization of the BBT, TQ and PQ polymers

Polymer	HOMO <sup>a</sup> / eV	LUMO <sup>a</sup> / eV	CV E <sub>g</sub> <sup>b</sup> / eV	Soln opt. E <sub>g</sub> <sup>b</sup> /eV	Thin film opt. E <sub>g</sub> <sup>c</sup> /eV	λ <sub>max</sub> , Soln <sup>b</sup> /nm	λ <sub>max</sub> Thin film <sup>c</sup> /nm	M <sub>w</sub> <sup>d</sup> × 10 <sup>4</sup> / g mol <sup>-1</sup>	PDI
pBBTF	-5.08	-4.00	1.08	1.27	1.06	359, 415, 759	364, 422, 848	1.41	1.89
pTQ1F	-5.19	-3.92	1.27	1.33	1.28	305, 428, 788	307, 437, 846	1.57	1.65
pTQ2F	-5.16	-3.98	1.18	1.30	1.23	362, 443, 817	367, 445, 877	2.08	1.72
pPQ1F	-5.32	-3.52	1.80	1.55	1.44	308, 405, 498, 657	308, 418, 512, 719	2.08	1.36
pPQ2F	-5.52	-3.72	1.80	1.45	1.37	357, 424, 621, 754s	363, 429, 641, 811s	2.16	1.34

<sup>a</sup> Measured by CV. <sup>b</sup> Measured in CHCl<sub>3</sub>. <sup>c</sup> Spincoated on glass. <sup>d</sup> Measured by GPC against polystyrene standard.

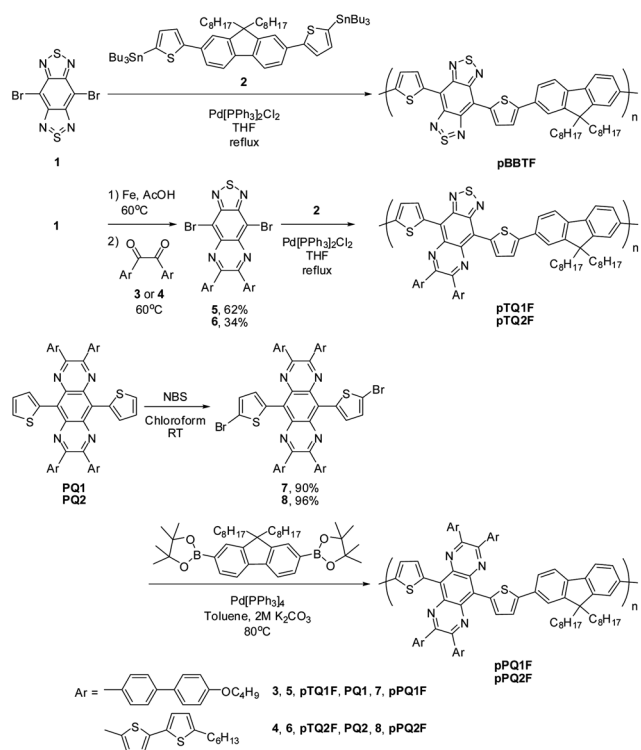
these molecules with **2** yielded the two polymers **pTQ1F** and **pTQ2F**. The dibromo derivatives of **BBT**, **TQ1** and **TQ2** were found to have limited solubilities and hence are not used for polymerization (Fig. 1). For the syntheses of PQ polymers, bromination of **PQ1** and **PQ2** using NBS in chloroform first yielded the monomers **7** and **8** respectively. Suzuki coupling of these with 9,9-dioctylfluorene-2,7-bis(boronic acid pinacol ester) yielded **pPQ1F** and **pPQ2F**, respectively.

The molecular weight of the polymers (Table 1) is modest and may be capable of optimization, *e.g.* through use of different catalysts or microwave heating. The syntheses of these polymers are shown in Scheme 1, and details of their physical and electrochemical characterization data can be found in Table 1. Optical bandgaps were calculated from the edges of absorption in the UV-Visible spectra which are shown in Fig. 2. There is excellent agreement between the solid state optical and electrochemical bandgaps for the polymers with exceptions in the case of polymers **pPQ1F** and **pPQ2F**. Geometry optimized structures of the dithienyl BBT, TQs and PQs, together with their

calculated HOMOs and LUMOs, can be found in Fig. 3. The calculated values for PQs have been previously reported by us,<sup>25</sup> whereas the values for the TQs were derived in the current work.

### Photophysical and electrochemical properties

All five polymers showed a low bandgap with absorption up to ~900 nm for **pPQ1F** and **pPQ2F** and ~1000 nm for **pBBTF**, **pTQ1F** and **pTQ2F** in thin films (Fig. 2b). As expected, the bandgaps of the polymers are in the order BBT < TQ < PQ due to stronger intramolecular charge transfer arising from stronger electron accepting nature and quinoid forming ability.<sup>14,26,27</sup> **pTQ2F** and **pPQ2F** also showed a slightly lower bandgap than **pTQ1F** and **pPQ1F** respectively due to the higher conjugation of the bithienyls as compared to the biphenyls.<sup>25</sup> The different substituents on TQ did not cause any significant change in the energy levels for the TQ polymers. However, a more pronounced



**Scheme 1** Syntheses of BBT, TQ and PQ polymers.

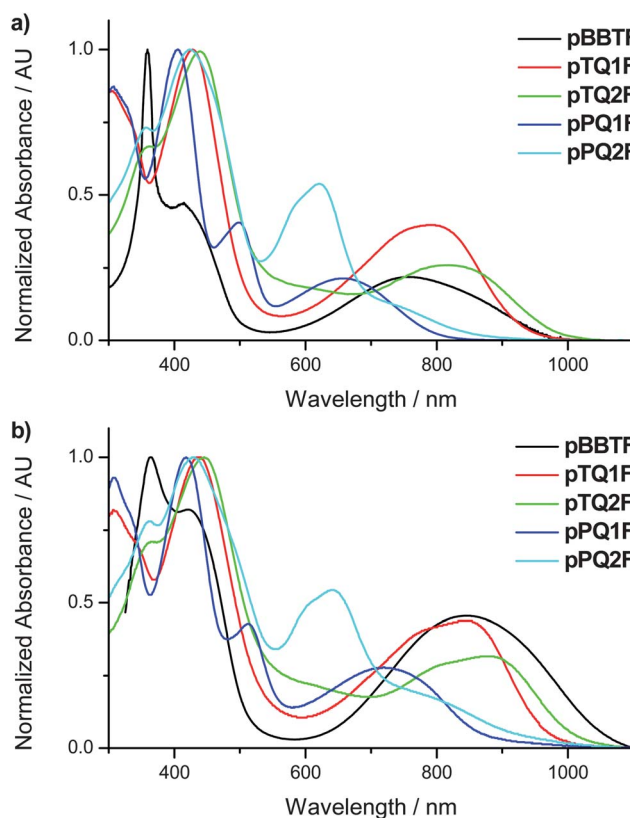


**Fig. 2** (a) Solution (chloroform) and (b) thin film (glass slide) UV-Vis-NIR absorption spectra of BBT, TQ and PQ polymers.

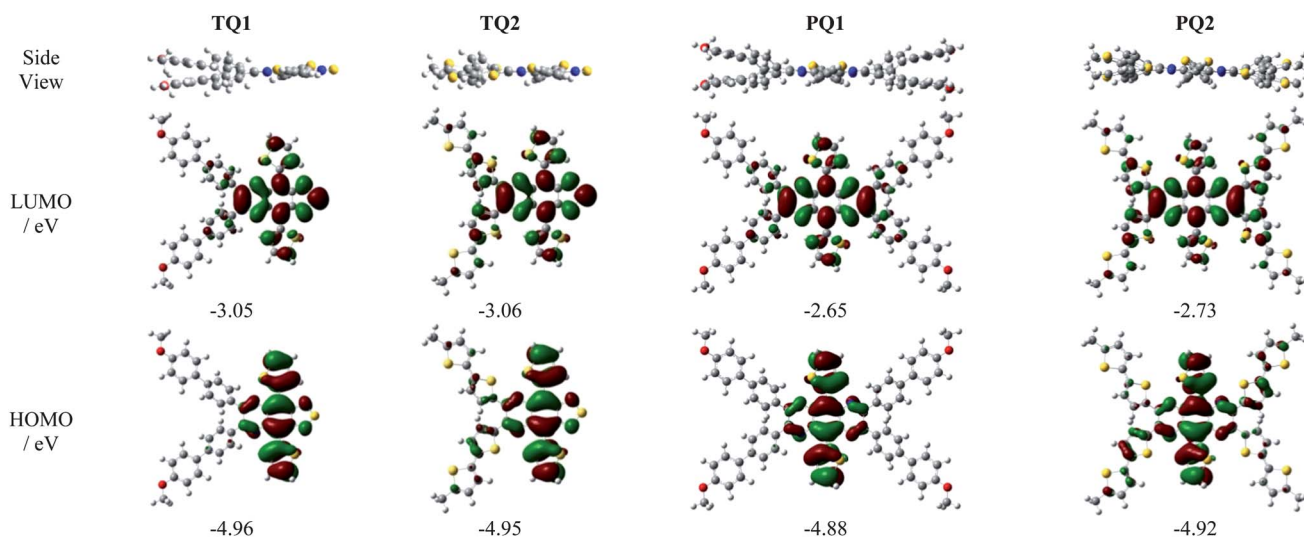


Fig. 3 DFT modeling of the TQ and PQ units using the B3LYP functional and 6-31G\* basis set under the geometry optimization conditions.

effect on the absorption spectra was easily seen from the less obvious valley at  $\sim 600$  nm for **pTQ2F** as compared to **pTQ1F**. The same trend was observed for the absorption spectra of **pPQ2F** and **pPQ1F** respectively. On the other hand, the different substituents on PQ did cause significant change in the energy levels for PQ polymers. This is because the bithienyls now induce a larger torsional strain on the thiophenes at the quinoid positions than the biphenyls, and have larger contribution in the HOMO and LUMO in PQ than TQ, as shown in the density functional theory (DFT) in Fig. 3. Together with the inherent weaker quinoid character of PQ as compared to TQ, these resulted in a stronger substituent effect on the energy levels for the PQ polymers.

From solution to thin film, UV-Vis-NIR absorption spectra (Fig. 2a and b) show insignificant bathochromic shifts for all the polymers at short wavelengths while higher shifts were observed at longer wavelengths. The BBT polymer showed the largest bathochromic shift of 89 nm while TQ and PQ polymers showed similar shifts from 57–62 nm. This higher bathochromic shift of **pBBTF** indicates that a higher aggregation of the polymer occurs in the solid state as compared to the TQ and PQ polymers.

### Thin film XRD

The aromatic substituents, together with the alkyl groups, can affect the packing of the polymers by changing the interchain and  $\pi$ - $\pi$  stacking distance. Thus XRD of the polymer thin films was measured as shown in Fig. 4. For **pBBTF**, the lack of these side groups and strong intermolecular S–N contacts allow individual polymer chains to come close together. Thus **pBBTF** showed a short interchain distance of 9.78 Å. Interestingly, no significant  $\pi$ - $\pi$  stacking was observed, as one would expect highly planar polymer chains of **pBBTF** to show strong  $\pi$ - $\pi$  stacking. Such an observation was previously reported by Yuen *et al.* for other BBT polymers.<sup>28,29</sup> Though we did not manage to obtain in-plane XRD for all of the polymers, we suspect that an edge-on configuration was generally present in BBT polymers which would account for their reported high charge mobilities.

The TQ polymers displayed interchain distances of 16.61 Å and 10.26 Å for **pTQ1F** and 21.76 Å and 10.14 Å for **pTQ2F** while the PQ polymers showed 22.77 Å and 8.21 Å for **pPQ1F** and 27.27 Å and 10.09 Å for **pPQ2F**. Due to the asymmetric nature of TQ units, there are three ways where the TQ polymers can arrange themselves: (1) head–head (thiadiazole–thiadiazole), (2) head–tail (thiadiazole–side groups) and (3) tail–tail (side groups–side groups). With reference to the polymers of symmetrical BBT and PQ units, the largest interchain distances for the TQ polymers should be a consequence of head–tail stacking since they are smaller than that of the PQ polymers, while the almost constant second interchain distance should be a result of head–head interaction for the TQ polymers since they match well with that of the BBT polymer. Such a head–head interaction has been observed previously in a TQ small molecule.<sup>30</sup>

Both TQ and PQ polymers showed a significant  $\pi$ - $\pi$  stacking signal as compared to BBT polymers, which might suggest larger tilt or face-on configuration. This is in contrast with the TQ–acetylene based polymers reported by Dallos *et al.* in which no clear indication of  $\pi$ - $\pi$  stacking was noticeable.<sup>31</sup> From TQ to PQ polymers, the increasing torsional strain between the

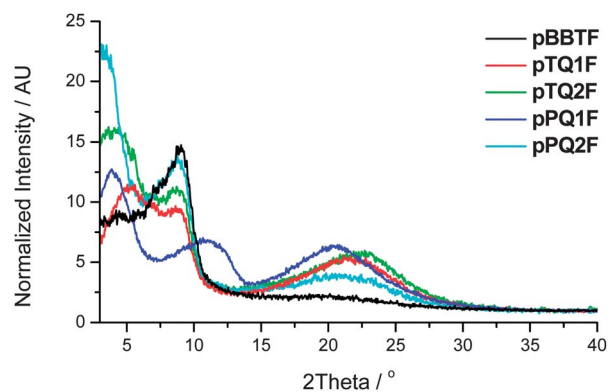


Fig. 4 Out-of-plane thin film XRD of BBT, TQ and PQ polymers dropcast from 1,2-dichlorobenzene on the SiO<sub>2</sub>/Si substrate. The data were normalized at the baseline.

**Table 2** Interchain and  $\pi$ - $\pi$  stacking distances and their intensities and intensity ratio of  $\pi$ - $\pi$  stacking/interchain

Polymer	Interchain distance/Å (intensity, $I_{ID}$ )	$\pi$ - $\pi$ stacking distance/Å (intensity, $I_{SD}$ )	$I_{SD}/I_{ID}$
pBBTF	9.78 (14.11)	—	—
pTQ1F	16.61 (11.11)	4.10 (5.24)	0.472
pTQ2F	21.76 (15.87)	3.96 (5.64)	0.355
pPQ1F	22.77 (12.34)	4.35 (6.27)	0.508
pPQ2F	27.27 (22.46)	4.26 (3.83)	0.171

aromatic substituents and the thiophenes at the quinoidal positions (see side view images of the TQ and PQ units in Fig. 3) prevents polymer chains from packing closely together, resulting in larger  $\pi$ - $\pi$  stacking distances for PQ (pPQ1F – 4.35 Å, pPQ2F – 4.26 Å) as compared to TQ polymers (pTQ1F – 4.10 Å, pTQ2F – 3.96 Å).

The XRD pattern of a PQ small molecule (PQ1a in the ESI, Fig. S1†) that resembled a part of the monomer unit of pPQ1F showed similarity when the X-ray incident beam was vertical to the nanowires, with strong signals from the (001), and (210), (223) and (213) planes.<sup>32</sup> The (001) plane corresponded to the intermolecular distance in the *c*-axis direction, while the (210), (223) and (213) planes corresponded more or less to the  $\pi$ - $\pi$  stacking directions. When the X-ray beam was parallel to the nanowires, the XRD pattern showed the absence of these  $\pi$ - $\pi$  stacking signals, indicating that the PQ small molecule was parallel to the X-ray beam. The vertical and parallel X-ray beam configurations resemble that of the out-of-plane and in-plane XRD. Inferring from these data, we can conclude that pPQ1F adopts a predominant face-on configuration on SiO<sub>2</sub>/Si. The crystal structure of PQ1a was said to be applicable to PQ2a<sup>32</sup> which resembled a part of the monomer unit of pPQ2F (see ESI Fig. S1†). Comparing with the XRD pattern of PQ2a (see ESI of ref. 23), we thus conclude that pPQ2F adopts a predominant edge-on configuration on SiO<sub>2</sub>/Si.

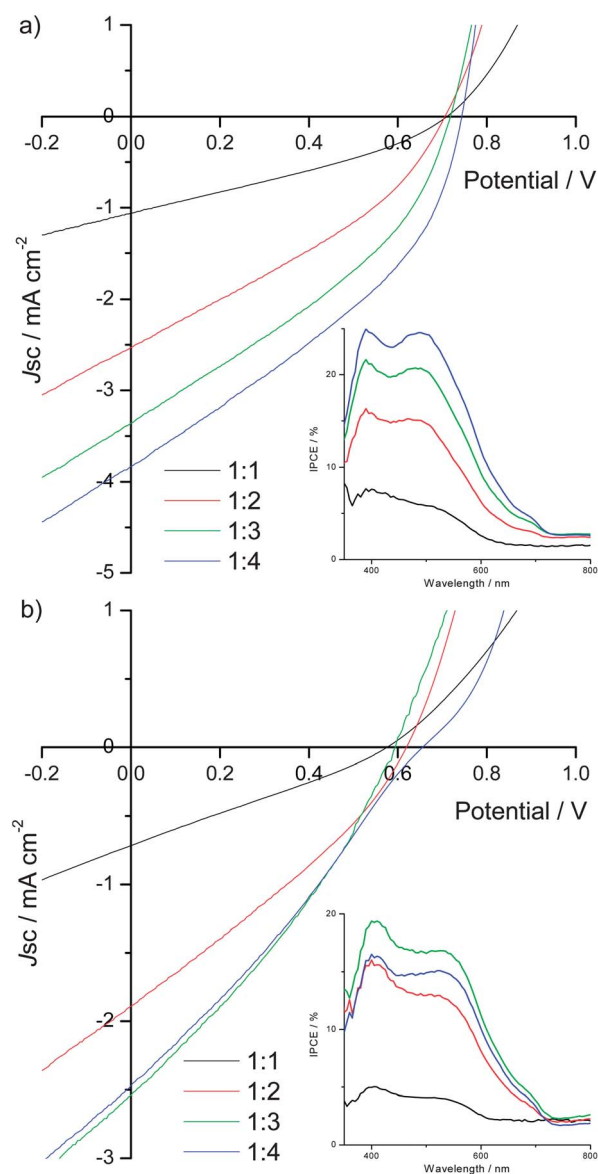
The intensity ratio of  $\pi$ - $\pi$  stacking and interchain distance of TQ and PQ polymers were calculated and tabulated in Table 2. This ratio gives a qualitative picture of the polymer/molecular orientation<sup>33,34</sup> of the  $\pi$ - $\pi$  stacking with respect to the interchain direction. As shown, pPQ1F showed the highest  $I_{SD}/I_{ID}$ , followed by pTQ1F, pTQ2F and pPQ2F. It seems that the conjugated side groups have an effect on either the preferential orientation of the polymer on the substrate or organization of the polymer chains.

**Table 3** Device performance of TQ polymers

Polymer	D/A ratio	Thickness /nm	$J_{sc}/\text{mA cm}^{-2}$	$V_{oc}/\text{V}$	FF	PCE/%
pTQ1F	1 : 1	~70	-1.06	0.71	0.32	0.24
	1 : 2	~70	-2.53	0.71	0.33	0.59
	1 : 3	~70	-3.36	0.72	0.35	0.85
pTQ2F	1 : 4	~60	-3.83	0.74	0.37	1.05
	1 : 1	~50	-0.72	0.58	0.27	0.11
	1 : 2	~50	-1.89	0.62	0.30	0.35
pTQ2F	1 : 3	~40	-2.54	0.59	0.31	0.47
	1 : 4	~40	-2.47	0.66	0.28	0.45

## OPV device characterization

The optimum device results, together with the  $J$ - $V$  and IPCE curves of TQ and PQ polymers are shown in Table 3, Fig. 5 and 8, respectively. pBBTF exhibited poor solubility and due to the low LUMO which reduces efficiency of electron transfer to the acceptor, showed very poor device performance ( $J_{sc} = 0.08 \text{ mA cm}^{-2}$ ,  $V_{oc} = 0.42 \text{ V}$ , FF = 0.25, PCE = 0.0086%). As noted above, pBBTF also may have a preference towards an edge-on orientation on substrates which is not favorable for vertical charge transport in OPV devices. On the other hand, the TQ polymers showed much better device performance. pTQ1F achieved a PCE of 1.05% at donor : acceptor (D : A) ratio of 1 : 4 while pTQ2F achieved a PCE of 0.51% at D : A ratio of 1 : 3. To the best of our knowledge, pTQ1F thus displays the highest PCE yet recorded for TQ based alternating copolymers in such standard device architectures without use of additives or of an electron transport/hole blocking layer.

**Fig. 5**  $J$ - $V$  curve and IPCE (inset) of (a) pTQ1F and (b) pTQ2F devices.

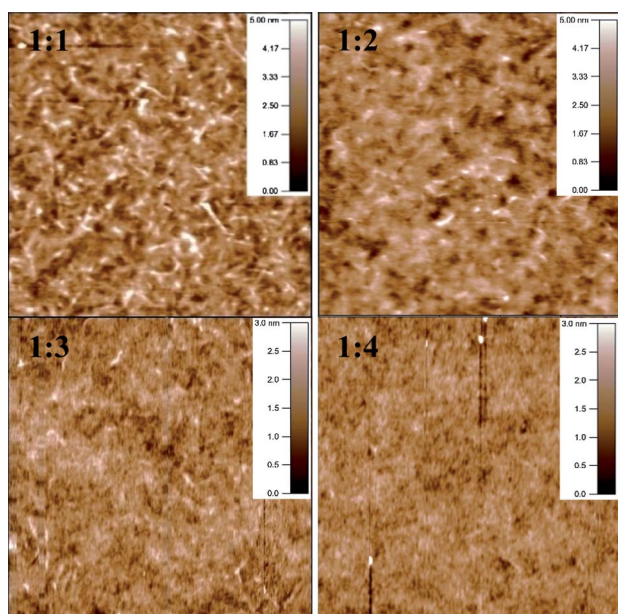


**Fig. 6** AFM images of non-annealed **pTQ1F** and PC[71]BM active layer on an actual device. The scan area is  $5 \mu\text{m} \times 5 \mu\text{m}$ .

AFM images showed smooth surfaces for thin films of all D/A ratios and annealing conditions for both TQ polymers, with **pTQ1F** showing nanofibre-like morphology (see Fig. 6) and **pTQ2F** showing fine morphology (see Fig. 7). **pTQ1F** showed higher  $J_{\text{sc}}$ ,  $V_{\text{oc}}$  and FF with respect to **pTQ2F** and these likely resulted from (1) higher mobility due to a shorter interchain distance, shorter  $\pi$ - $\pi$  stacking distance and higher ratio of face-on configuration, (2) a better percolation pathway through a nanofibre-like morphology, (3) a higher energy offset to overcome the binding energy of the exciton due to the higher LUMO and (4) the deeper HOMO resulting in higher  $V_{\text{oc}}$ . As the ratio of

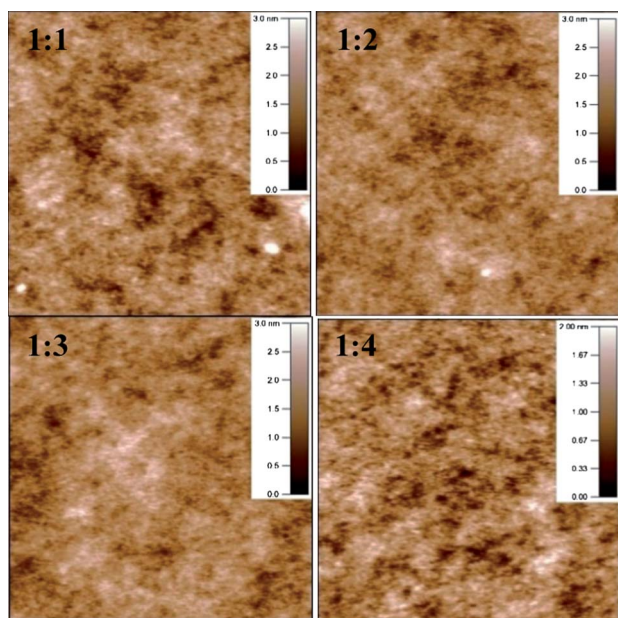


**Fig. 7** AFM images of non-annealed **pTQ2F** and PC[71]BM active layer on an actual device. The scan area is  $5 \mu\text{m} \times 5 \mu\text{m}$ .

**Table 4** Device performance of PQ polymers

Polymer	D/A ratio	Thickness/ nm	$J_{\text{sc}}/$ $\text{mA cm}^{-2}$	$V_{\text{oc}}/$ V	FF	PCE/%
<b>pPQ1F</b>	1 : 1	~100	-4.06	0.84	0.31	1.05
	1 : 2	~90	-6.44	0.83	0.37	1.97
	1 : 3	~90	-7.35	0.82	0.39	2.36
	1 : 4	~90	-6.95	0.82	0.36	2.05
<b>pPQ2F</b>	1 : 1	~50	-0.35	0.35	0.25	0.031
	1 : 2	~50	-0.46	0.25	0.26	0.030
	1 : 3	~50	-0.51	0.29	0.26	0.038
	1 : 4	~40	-0.39	0.22	0.27	0.023

PC[71]BM increases, the nanofibre-like morphology disappears, replaced by the fine morphology. This suggests that the surface of the blend may have changed from **pTQ1F** rich to PC[71]BM rich, which results in better extraction of electrons and lower recombination as suggested by the increasing  $J_{\text{sc}}$  and FF. Besides, the higher PC[71]BM content also promotes more percolation pathways for electron transport. This results in a more balanced charge transport between holes and electrons, reducing series resistance of the device (or higher FF). However, the width of the nanofiber appeared to be around 100 nm, which is too large for the exciton to diffuse to the donor-acceptor interface, thus limiting the performance of **pTQ1F**. Proper morphological control of the nanofiber dimensions (to 10–20 nm) may improve exciton dissociation prior to recombination, generating more free-carriers; hence, better solar cell devices.

In the case of PQ polymers, there was a drastic contrast in the device performance between **pPQ1F** and **pPQ2F** (Table. 4). **pPQ1F** achieved a high PCE of 2.36% at D : A ratio of 1 : 3 with a high  $J_{\text{sc}}$  of  $7.35 \text{ mA cm}^{-2}$ , a high  $V_{\text{oc}}$  of 0.82 V and a low FF of 0.39 (Fig. 8). On the other hand, **pPQ2F** only managed to give a PCE of 0.038% with a very low  $J_{\text{sc}}$ ,  $V_{\text{oc}}$  and FF after optimization. Energetically speaking, **pPQ2F** has suitable HOMO and LUMO levels to be used as a donor material with PC[71]BM. The surprising device performance prompted a possible issue in the morphology of the active layer and/or active layer-electrode

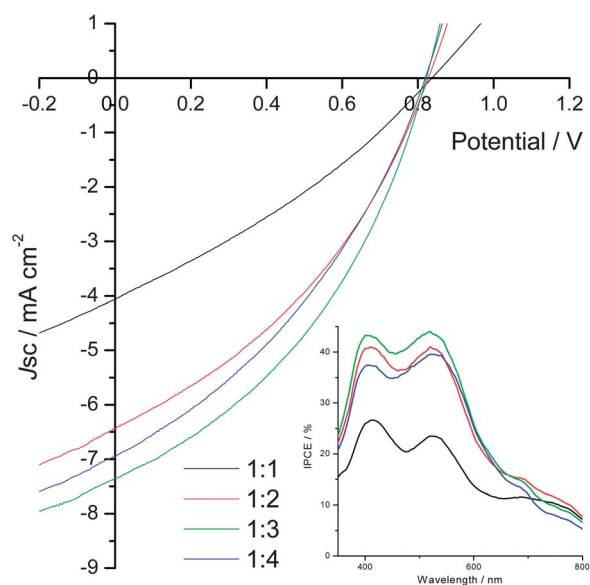


**Fig. 8**  $J$ - $V$  curve and IPCE (inset) of **pPQ1F** devices.

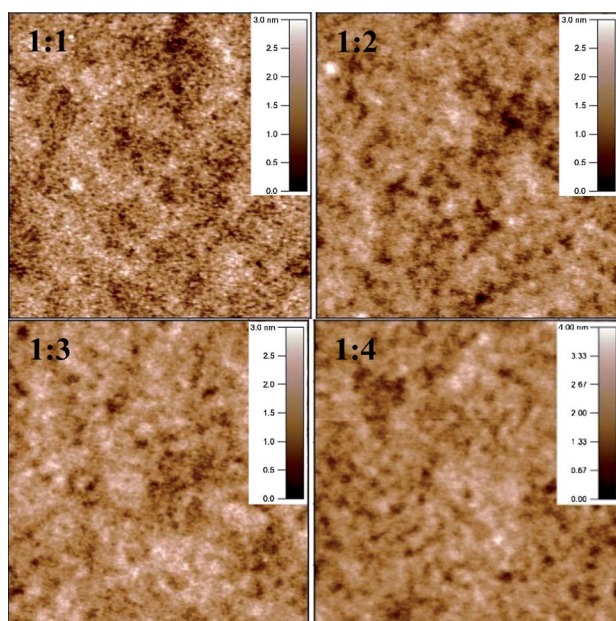


**Fig. 9** AFM images of non-annealed **pPQ1F** and PC[71]BM active layer. The scan area is  $5 \mu\text{m} \times 5 \mu\text{m}$ .

interface. However the AFM images show smooth surfaces for both PQ polymers, with **pPQ1F** showing very fine features (see Fig. 9) while **pPQ2F** showing very large features of more than 500 nm in the morphology (see Fig. 10). The fine features of **pPQ1F** help to maximize exciton dissociation *via* nanoscale phase separation between the donor and acceptor interface while the large features of **pPQ2F** do not. The shorter interchain distance, shorter  $\pi$ - $\pi$  stacking distance and the higher ratio of face-on configuration for **pPQ1F** are likely to produce better charge transport which will further boost the efficiency of the

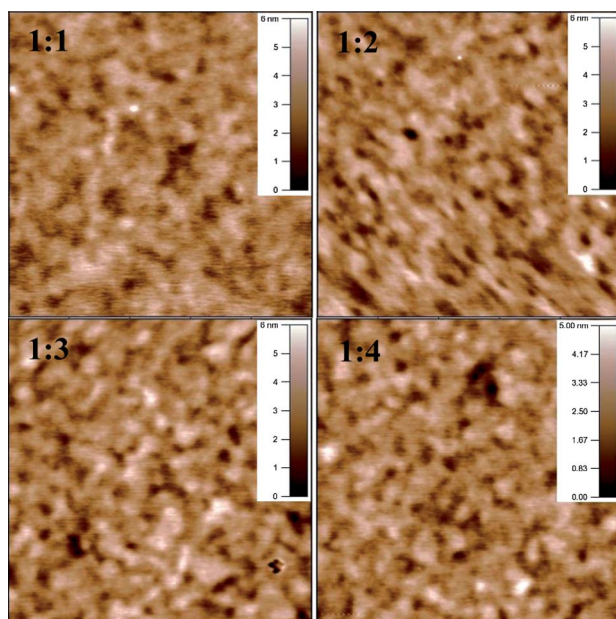


**Fig. 10** AFM images of non-annealed **pPQ2F** and PC[71]BM active layer. The scan area is  $5 \mu\text{m} \times 5 \mu\text{m}$ .

device. Likewise, the edge-on configuration of **pPQ2F** may have contributed to the low  $J_{\text{sc}}$ . However, these do not fully explain the low  $V_{\text{oc}}$  of **pPQ2F** devices.

It was reported that the kinetics of recombination at the D-A interfaces have a strong impact on the  $V_{\text{oc}}$ .<sup>35</sup> Materials with sterically inaccessible  $\pi$ -systems and non-planar geometries can kinetically suppress dark recombination processes, represented by the reverse saturation current density ( $J_0$ ).<sup>35-37</sup> Under open circuit conditions,  $V_{\text{oc}}$  is correlated with  $J_0$  from the following relationship:<sup>37</sup>

$$V_{\text{oc}} \approx \frac{nkT}{q} \ln \left( \frac{J_{\text{sc}}}{J_0} \right)$$

Therefore, D-A systems with suppressed  $J_0$  tend to have a higher  $V_{\text{oc}}$ . The dark  $J$ - $V$  characteristics of **pPQ1F** : PC[71]BM (1 : 3) and **pPQ2F** : PC[71]BM (1 : 3) were exponentially fitted (Fig. 11) to extract  $J_0$  values of  $3.6 \times 10^{-9} \text{ mA cm}^{-2}$  and  $8.6 \times 10^{-4} \text{ mA cm}^{-2}$ , respectively. The five orders of magnitude difference in  $J_0$  is represented as the remarkably lower  $V_{\text{oc}}$  in **pPQ2F** : PC[71]BM devices. The shunt effect can also be

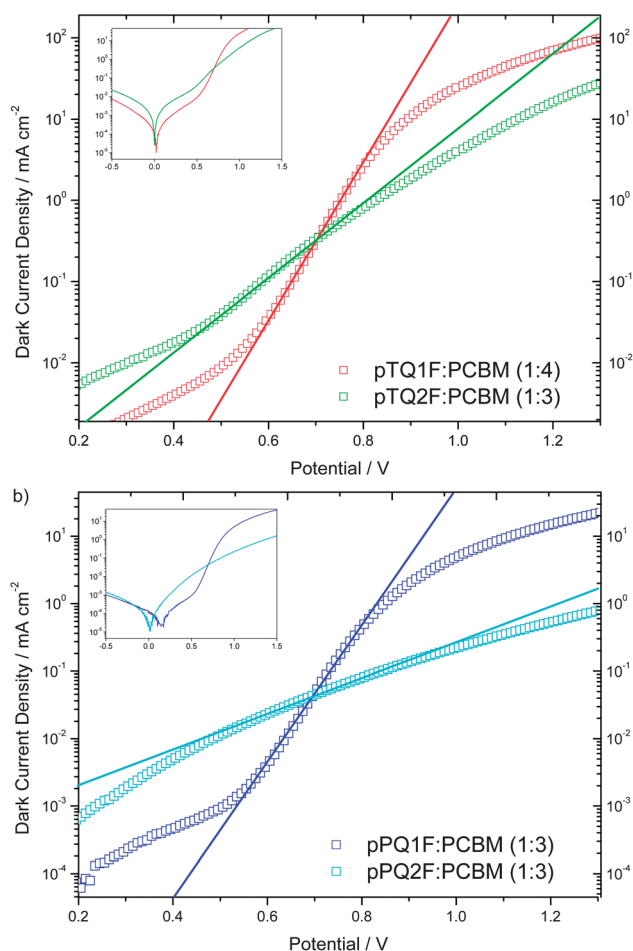


**Fig. 11** Dark current density-voltage ( $J$ - $V$ ) characteristics of (a) **pTQ1F** : PC[71]BM (1 : 4) and **pTQ2F** : PC[71]BM (1 : 3) and (b) **pPQ1F** : PC[71]BM (1 : 3) and **pPQ2F** : PC[71]BM (1 : 3) devices. The solid lines are the exponential fits to the  $J$ - $V$  characteristics at the intermediate voltages. The inset shows the same curves over a wider range of voltages.

excluded as both devices give comparable shunt resistance ( $R_{sh}$ ) of  $3.1 \times 10^{-2}$  and  $5.7 \times 10^{-2} \Omega \text{ cm}^2$ . This also suggests that the higher  $J_0$  indicates stronger interactions of the  $\pi$ -conjugated molecules in the **pPQ2F**:PC[71]BM blend.<sup>37</sup> Comparison of bithienyl and biphenyl substituents reveals that the former is likely to allow darker recombination processes due to higher planarity with the core, and hence much lower  $V_{oc}$  than expected in **pPQ2F** devices. This is also supported by the presence of large features in the **pPQ2F**:PC[71]BM blend surface, as planarity promotes molecular aggregation. Despite the lack of coplanarity of the substituents to the core in the **pPQ1F** system, no detrimental effects were observed on both exciton diffusion and charge transport processes, as evidenced from the higher  $J_{sc}$  and FF in **pPQ1F**:PC[71]BM devices. The same reasoning can be used to explain why **pTQ2F** ( $J_0 = 9.4 \times 10^{-5} \text{ mA cm}^{-2}$ ) shows almost 0.1 V lower in  $V_{oc}$  as compared to **pTQ1F** ( $J_0 = 2.2 \times 10^{-8} \text{ mA cm}^{-2}$ ) when both of them have similar HOMO energy levels.

## Conclusion

In conclusion, we have demonstrated the effects of aromatic substituents on the photophysical properties, morphology and OPV device performance of BBT, TQ and PQ polymers. The bithienyls in **pTQ2F** and **pPQ2F** offer a lower bandgap and broader light absorption *via* higher conjugation as compared to the biphenyls in **pTQ1F** and **pPQ1F**. Even though these properties are generally beneficial for device performance, they are at the expense of a higher HOMO and a larger dark current which result in a lower  $V_{oc}$ , and lower LUMO which provides a lesser driving force to overcome exciton binding energy. The lower ratio of face-on configuration and the higher reverse saturation current in the former also appear to be more detrimental to the device performance in terms of the lower  $J_{sc}$  and  $V_{oc}$ , respectively. These results provide some insight into polymeric materials with conjugated side chains for OPV applications and also help in the design of new materials with low bandgap and broad light absorption.

## Acknowledgements

This work was supported financially by Robert Bosch (SEA) Pte Ltd. We would like to thank Miss Fan Shufen, Miss Tay Qiuling, and Miss Liu Weiling (NTU MSE) for helpful discussions on the XRD results.

## Notes and references

- C. Winder and N. S. Sariciftci, *J. Mater. Chem.*, 2004, **14**, 1077–1086.
- E. Bundgaard and F. C. Krebs, *Sol. Energy Mater. Sol. Cells*, 2007, **91**, 954–985.
- R. Kroon, M. Lenes, J. C. Hummelen, P. W. M. Blom and B. d. Boer, *Polym. Rev.*, 2008, **48**, 531–582.
- J. Chen and Y. Cao, *Acc. Chem. Res.*, 2009, **42**, 1709–1718.
- M. Helgesen, R. Søndergaard and F. C. Krebs, *J. Mater. Chem.*, 2010, **20**, 36–60.
- W. Cai, X. Gong and Y. Cao, *Sol. Energy Mater. Sol. Cells*, 2010, **94**, 114–127.
- Y. Li and Y. Zou, *Adv. Mater.*, 2008, **20**, 2952–2958.
- Y.-J. Cheng, S.-H. Yang and C.-S. Hsu, *Chem. Rev.*, 2009, **109**, 5868–5923.
- J. Roncali, *Macromol. Rapid Commun.*, 2007, **28**, 1761–1775.
- J. Hou, Z. a. Tan, Y. He, C. Yang and Y. Li, *Macromolecules*, 2006, **39**, 4657–4662.
- J. Hou, Z. a. Tan, Y. Yan, Y. He, C. Yang and Y. Li, *J. Am. Chem. Soc.*, 2006, **128**, 4911–4916.
- Y. Zou, W. Wu, G. Sang, Y. Yang, Y. Liu and Y. Li, *Macromolecules*, 2007, **40**, 7231–7237.
- E. Zhou, Z. a. Tan, L. Huo, Y. He, C. Yang and Y. Li, *J. Phys. Chem. B*, 2006, **110**, 26062–26067.
- H. Li, T. L. Tam, Y. M. Lam, S. G. Mhaisalkar and A. C. Grimsdale, *Org. Lett.*, 2011, **13**, 46–49.
- X. Zhang, Z. a. Tan, T. Steckler, R. R. Dasari, S. Ohira, W. J. Potscavage Jr, S. P. Tiwari, S. Coppée, S. Ellinger, S. Barlow, J.-L. Brédas, B. Kippelen, J. R. Reynolds and S. R. Marder, *J. Mater. Chem.*, 2010, **20**, 123–134.
- M. Chen, X. Crispin, E. Perzon, M. R. Andersson, T. Pullerits, M. Andersson, O. Inganäs and M. Berggren, *Appl. Phys. Lett.*, 2005, **87**, 252105.
- X. Wang, E. Perzon, F. Oswald, F. Langa, S. Admassie, M. R. Andersson and O. Inganäs, *Adv. Funct. Mater.*, 2005, **15**, 1665–1670.
- E. Perzon, F. Zhang, M. Andersson, W. Mammo, O. Inganäs and M. R. Andersson, *Adv. Mater.*, 2007, **19**, 3308–3311.
- A. P. Zoombelt, M. Fonrodona, M. M. Wienk, A. B. Sieval, J. C. Hummelen and R. A. J. Janssen, *Org. Lett.*, 2009, **11**, 903–906.
- Y. Lee, T. P. Russell and W. H. Jo, *Org. Electron.*, 2010, **11**, 846–853.
- F. Zhang, J. Bijleveld, E. Perzon, K. Tvingstedt, S. Barrau, O. Inganäs and M. R. Andersson, *J. Mater. Chem.*, 2008, **18**, 5468–5474.
- A. P. Zoombelt, M. Fonrodona, M. G. R. Turbiez, M. M. Wienk and R. A. J. Janssen, *J. Mater. Chem.*, 2009, **19**, 5336–5342.
- E. Wang, L. Hou, Z. Wang, S. Hellstrom, W. Mammo, F. Zhang, O. Inganäs and M. R. Andersson, *Org. Lett.*, 2010, **12**, 4470–4473.
- T. L. Tam, H. Li, F. Wei, K. J. Tan, C. Kloc, Y. M. Lam, S. G. Mhaisalkar and A. C. Grimsdale, *Org. Lett.*, 2010, **12**, 3340–3343.
- T. L. Tam, F. Zhou, H. Li, J. C. Y. Pang, Y. M. Lam, S. G. Mhaisalkar, H. Su and A. C. Grimsdale, *J. Mater. Chem.*, 2011, **21**, 17798–17804.
- C.-L. Pai, C.-L. Liu, W.-C. Chen and S. A. Jenekhe, *Polymer*, 2006, **47**, 699–708.
- W.-C. Wu and W.-C. Chen, *J. Polym. Res.*, 2006, **13**, 441–449.
- J. D. Yuen, J. Fan, J. Seifter, B. Lim, R. Hufschmid, A. J. Heeger and F. Wudl, *J. Am. Chem. Soc.*, 2011, **133**, 20799–20807.
- J. D. Yuen, R. Kumar, D. Zakhidov, J. Seifter, B. Lim, A. J. Heeger and F. Wudl, *Adv. Mater.*, 2011, **23**, 3780–3785.
- S. Miao, P. v. R. Schleyer, J. I. Wu, K. I. Hardcastle and U. H. F. Bunz, *Org. Lett.*, 2007, **9**, 1073–1076.
- T. Dallos, D. Beckmann, G. Brunklaus and M. Baumgarten, *J. Am. Chem. Soc.*, 2011, **133**, 13898–13901.
- X. Wang, Y. Zhou, T. Lei, N. Hu, E.-Q. Chen and J. Pei, *Chem. Mater.*, 2010, **22**, 3735–3745.
- W. Porzio, G. Scavia, L. Barba, G. Arrighetti and S. Milita, *Eur. Polym. J.*, 2011, **47**, 273–283.
- E. Orgiu, A. M. Masillamani, J.-O. Vogel, E. Treossi, A. Kiersnowski, M. Kastler, W. Pisula, F. Dötz, V. Palermo and P. Samorì, *Chem. Commun.*, 2012, **48**, 1562–1564.
- C. W. Schlenker and M. E. Thompson, *Chem. Commun.*, 2011, **47**, 3702–3716.
- P. Erwin and M. E. Thompson, *Appl. Phys. Lett.*, 2011, **98**, 223305.
- M. D. Perez, C. Borek, S. R. Forrest and M. E. Thompson, *J. Am. Chem. Soc.*, 2009, **131**, 9281–9286.